Journal of Power Sources 235 (2013) 193–201

Contents lists available at SciVerse ScienceDirect

Journal of Power Sources

journal homepage: www.elsevier.com/locate/jpowsour

Optimization of single-crystal rutile TiO_2 nanorod arrays based dye-sensitized solar cells and their electron transport properties

Shi-Mao Wang [a], Wei-Wei Dong [a,b,*], Ru-Hua Tao [a,b], Zan-Hong Deng [a,b], Jing-Zhen Shao [a], Lin-Hua Hu [b], Jun Zhu [b], Xiao-Dong Fang [a,b,c,*]

[a] Anhui Provincial Key Laboratory of Photonic Devices and Materials, Anhui Institute of Optics and Fine Mechanics, Chinese Academy of Sciences, Hefei 230031, PR China
[b] Key Lab of Novel Thin Film Solar Cells, Chinese Academy of Sciences, P.O. Box 1126, Hefei, Anhui 230031, PR China
[c] School of Environmental Science and Photoelectric Technology, University of Science and Technology of China, Hefei 230026, PR China

HIGHLIGHTS

- $TiCl_4$ modification of TiO_2 nanorod arrays based DSSCs (TNRs-DSSCs) was optimized.
- TNRs-DSSCs obtained relatively high energy conversion efficiency (η) of 4.14 ± 0.07%.
- Compared to P25 based DSSCs, TNRs-DSSCs with a fifth of dye could obtain similar η.
- TNRs-DSSCs have a comparable charge-collection efficiency with P25 based DSSCs.

ARTICLE INFO

Article history:
Received 1 August 2012
Received in revised form
16 November 2012
Accepted 16 January 2013
Available online 6 February 2013

Keywords:
Dye-sensitized solar cell
Titania nanorod arrays
Titanium tetrachloride modification
Dye adsorption
Charge-collection efficiency

ABSTRACT

$TiCl_4$ solution growth has been introduced to modify the single-crystal rutile TiO_2 nanorod arrays (TNRs) used as photoanodes of dye-sensitized solar cells (DSSCs). After modification, a large number of rutile TiO_2 nanoparticles have been synthesized on the surface of TNRs. The surface area and dye adsorption of these modified TNRs increase obviously, and their photovoltaic performance improves significantly. The maximum energy conversion efficiency of 4.14 ± 0.07% has been obtained when the concentration of $TiCl_4$ solution is 0.2 M and the growth time is 36 h. To obtain similar energy conversion efficiencies the single-crystal TNRs based DSSCs need far less amount of dye than P25 TiO_2 nanoparticles based DSSCs. Contrary to previous publications, the electron transport rate of bare and modified single-crystal rutile TNRs with one-dimensional nanostructures is slower than that of P25 TiO_2 nanoparticles film. But the increase of the electron recombination lifetime of the bare and modified single-crystal rutile TNRs compensates for the slower electron transport rate, and makes them have similar charge-collection efficiencies to that of P25 TiO_2 nanoparticles based DSSCs.

1. Introduction

With the advantages of low-cost, pollution-free and relatively high energy conversion efficiency of about 12%, dye-sensitized solar cells (DSSCs) have attracted extensive research attention and become one of the most promising alternatives to Si-based photovoltaic cells in the latest two decades [1–5]. The conventional photoanodes of DSSCs are made from TiO_2 nanoparticles. When photogenerated electrons transfer in the nanoparticles photoanodes, electron scattering and trapping couldn't be avoided at grain boundaries [6], which would affect the performance of DSSCs. Thin films made of vertically aligned one-dimensional TiO_2 nanostructures, such as nanowire arrays, nanorod arrays and nanotube arrays, could provide un-interrupted electrical pathways for photogenerated electrons. These structures are proposed to increase the electron transport rate, and then improve the performance of DSSCs [7,8].

In recent years, several different approaches have been developed to grow single-crystal rutile TiO_2 nanorod/nanowire arrays directly on fluorine-doped tin oxide (FTO) glass and the prepared arrays were used as photoanodes of DSSCs [6,7,9–11]. However, the specific surface area of TiO_2 nanorod/nanowire arrays is much

* Corresponding authors. Anhui Provincial Key Laboratory of Photonic Devices and Materials, Anhui Institute of Optics and Fine Mechanics, Chinese Academy of Sciences, Hefei 230031, PR China. Tel.: +86 551 65593661; fax: +86 551 65593665.
E-mail addresses: wangshm@mail.ustc.edu.cn (S.-M. Wang), wwdong@aiofm.ac.cn (W.-W. Dong), rhtao@aiofm.ac.cn (R.-H. Tao), zhdeng@aiofm.ac.cn (Z.-H. Deng), jzshao@mail.ustc.edu.cn (J.-Z. Shao), solarhu@sina.com (L.-H. Hu), zhujzhu@gmail.com (J. Zhu), xdfang@aiofm.ac.cn (X.-D. Fang).

0378-7753/$ – see front matter © 2013 Elsevier B.V. All rights reserved.
http://dx.doi.org/10.1016/j.jpowsour.2013.01.106

lower than that of TiO_2 nanoparticles films, which leads to low dye adsorption and poor energy conversion efficiency. Solution growth technique using aqueous solution of $TiCl_4$ to synthesize TiO_2 nanostructures on TiO_2 nanorod arrays (TNRs) is an effective route to increase the specific surface area of TNRs. After solution growth, a large number of tiny TiO_2 crystallites or TiO_2 nano-branches [12] grew on nanorod surfaces, which would increase the specific surface area and dye adsorption of TNRs significantly, subsequently the performance of TNRs based DSSCs would be improved obviously. But the impact of the growth parameters on the morphology, dye adsorption and cell performance of TNRs has not been investigated in detail. Optimizing the parameters of $TiCl_4$ solution growth in depth would improve the performance of TNRs based DSSCs considerably.

The investigations about the electron transport properties of single-crystal rutile TNRs based DSSCs were reported only a few times [13–15]. In the investigation made by Enache-Pommer et al., the electron transport rate in DSSCs made from single-crystal rutile TNRs was found to be similar to that in DSSCs made from P25 TiO_2 nanoparticles [13]. Yang et al. found that single-crystal rutile TNRs have significantly better electron transport properties than rutile TiO_2 nanoparticles film [14]. However, most of the previous comparisons were carried out after single-crystal rutile TNRs and nanoparticles films were modified using $TiCl_4$ solution. After $TiCl_4$ modification, single-crystal rutile TiO_2 nanorods were covered with large number of TiO_2 crystallites, which would affect the electron transport and recombination obviously.

In our investigation, single-crystal rutile TNRs were synthesized directly on FTO glass through hydrothermal method developed by Liu and Aydil [6]. $TiCl_4$ solution with different concentrations (0.1 M and 0.2 M) was used to modify the prepared single-crystal rutile TNRs for different time. The bare and modified single-crystal rutile TNRs were used as photoanodes to assemble DSSCs. The electron transport and recombination behaviors in the bare and modified single-crystal rutile TNRs based DSSCs were analyzed using intensity modulated photocurrent spectroscopy (IMPS) [16–21] and intensity modulated photovoltage spectroscopy (IMVS) [17–20] respectively.

2. Experimental details

2.1. Synthesis of bare TNRs

TNRs were synthesized through a two-step hydrothermal process. Two different growth solutions named solution A and solution B were used in the two steps respectively. Deionized water and concentrated hydrochloric acid (37% by weight) were mixed with volume ratio of 1:1. After the mixture was stirred for 5 min, appropriate titanium butoxide (99% by weight, ACROS, USA) was added, and after stirring for another 5 min, 0.03 M titanium butoxide solution named solution A was obtained. In the process of preparing solution B, appropriate sodium chloride was introduced to the mixture of deionized water and concentrated hydrochloric acid and made the solution reach saturated for sodium chloride. The other operations were same to the preparation of solution A. The substrates of FTO glass were ultrasonically cleaned in acetone, absolute ethanol and deionized water respectively for 15 min. After dried in a nitrogen stream, the FTO substrates were placed against the wall of the Teflon-liner of a stainless steel autoclave (40 mL volume) with their conductive sides facing down. In the first step, 28 mL of solution A was transferred into the Teflon-liner and the hydrothermal synthesis was carried out at 150 °C for 4 h in an oven. In the second step, solution A was replaced with freshly prepared solution B, the reaction temperature was still 150 °C, and the hydrothermal synthesis lasted for 10 h. The second step was repeated for several times in order to increase the length of TiO_2 nanorods. After the second step, the samples were rinsed with deionized water and dried at 60 °C for 2 h in a furnace.

2.2. $TiCl_4$ modification of bare TNRs

The as-prepared TNRs were modified through solution growth method by immersing the samples in an aqueous solution of $TiCl_4$ for different time. The samples modified with 0.1 M $TiCl_4$ solution were immersed at room temperature for 12, 24, 36, 48, 60 and 72 h respectively, the others were immersed in 0.2 M $TiCl_4$ solution at room temperature for 12, 24, 36 and 48 h respectively. After immersion, the samples were rinsed with absolute ethanol, and then were annealed in air at 450 °C for 30 min inside a furnace. The samples' name and the modification parameters were listed in Table 1.

2.3. DSSCs assembly

The active area of the DSSCs was 0.25 cm^2. Before assembly, the bare and modified TNRs and the P25 TiO_2 nanoparticles films used as photoanodes were immersed in a 0.3 mM tert-butanol/acetonitrile (1:1) solution of dye N-719 [bis-tetrabutylammonium *cis*-bis(isothiocyanato) bis(2,2′-bipyridyl-4,4′-dicarboxylato) ruthenium(II)] at room temperature for 24 h. After they were rinsed with absolute ethanol and dried in a nitrogen stream, dye-sensitized photoanodes were obtained. The platinized FTO glass

Table 1
Modification parameters, the amount of adsorbed N719, roughness factor and photovoltaic parameters of bare single-crystal TNRs, modified single-crystal TNRs and P25 TiO_2 nanoparticles films.

Sample[a]	Thickness (μm)	Concn. of $TiCl_4$ solution (M)	Growth time (h)	Adsorbed N719 ($\times10^{-8}$ mol cm^{-2})	Roughness factor	V_{oc} (V)	J_{sc} (mA cm^{-2})	FF	η (%)
34-0	3.79 ± 0.04	–	–	1.00	96.15	0.76	1.47	0.46	0.52 ± 0.03
34-1-12	3.85 ± 0.06	0.1	12	0.60	57.69	0.74	2.16	0.61	0.98 ± 0.02
34-1-24	3.76 ± 0.07	0.1	24	0.80	76.92	0.74	4.68	0.67	2.30 ± 0.10
34-1-36	3.76 ± 0.05	0.1	36	1.02	98.08	0.78	7.00	0.57	3.11 ± 0.08
34-1-48	3.83 ± 0.04	0.1	48	1.55	149.04	0.77	7.56	0.62	3.60 ± 0.09
34-1-60	3.78 ± 0.04	0.1	60	2.03	195.19	0.76	8.95	0.59	4.01 ± 0.05
34-1-72	3.81 ± 0.06	0.1	72	2.47	237.50	0.76	8.17	0.62	3.85 ± 0.13
34-2-12	3.76 ± 0.04	0.2	12	0.68	65.38	0.79	3.05	0.52	1.25 ± 0.06
34-2-24	3.78 ± 0.03	0.2	24	1.42	136.54	0.80	5.48	0.54	2.35 ± 0.03
34-2-36	3.84 ± 0.04	0.2	36	1.90	182.69	0.76	9.03	0.60	4.14 ± 0.07
34-2-48	4.63 ± 0.12	0.2	48	2.61	250.96	0.72	6.84	0.63	3.09 ± 0.05
NP-0[b]	4.9 ± 0.2	–	–	8.76	842.31	0.73	8.12	0.69	4.07 ± 0.07

[a] In the hydrothermal synthesis of these samples, the second step was repeated three times, and the total reaction time was 34 h.
[b] A P25 TiO_2 nanoparticles film.

used as counter electrode was placed on the top of the dye-sensitized photoanode sealed with a 30-μm thick thermal adhesive film (Bynel, DuPont, USA). The electrolyte solution [0.6 M tetrapropylammonium iodide, 0.1 M iodine, 0.1 M lithium iodide, 0.5 M 4-tert-butylpyridine (TBP) in 3-methoxpropiponitrile] was filled into the space between the photoanode and the counter electrode from a hole made on the counter electrode using capillary action. In addition, the P25 TiO_2 nanoparticles (~70% anatase, ~30% rutile) based DSSCs were used to compare the electron transport properties of nanoparticles based DSSCs with that of single-crystal rutile TNRs based DSSCs. The P25 TiO_2 nanoparticles films were fabricated through screen-printing method, and the thickness of the film was 4.9 ± 0.2 μm.

2.4. Characterization

Morphologies of the bare and modified TNRs were characterized using a field-emission scanning electron microscope (FE-SEM, FEI Sirion-200, USA). Crystal structures were examined by X-ray diffraction (XRD) using a X-ray diffractometer (Philips X'pert, Holland) with Cu Kα radiation (λ = 1.5418 Å). Transmission electron microscopy (TEM), high-resolution TEM (HR-TEM) and selected-area electron diffraction (SAED) analyses were performed on a high-resolution transmission electron microscope (JEOL JEM-2010, Japan).

To estimate the amount of adsorbed dye N719 on different TiO_2 films and the roughness factor of different TiO_2 films, the sensitized electrodes were immersed in 10 mL of 0.2 M NaOH solution to desorb N719 from TiO_2 films respectively. The UV–visible absorption spectra of the resulting solutions were measured using a UV–vis spectrophotometer (HITACHI, U-3900H, Japan). UV–visible diffuse reflectance absorption spectra (UV–vis DRS) were used to compare light-harvesting efficiency of different samples [22,23]. The UV–vis DRS of the samples were measured using a UV–vis spectrophotometer (Shimadzu, SolidSpec-3700DUV, Japan), and $BaSO_4$ was used as a reflectance standard in the measurement.

The photocurrent–photovoltage (J–V) curves of DSSCs were derived with a Keithley 2420 digital source meter under irradiation of a solar simulator (Newport Oriel 94043A, USA, AM1.5, 100 mW cm^{-2}). The incident photon to current efficiency (IPCE) spectra was measured using 300 W Xe lamp light source with monochromatic light in the range of 250–800 nm. IMPS and IMVS measurements were carried out on an IM6ex electrochemical workstation (Zahner Company, Germany) using light-emitting diodes (λ = 610 nm) driven by Expot (Zahner Company, Germany). The LED provided both DC and AC components of the illumination. A small AC component was 10% or less than that of the DC component and the frequency range is 3 kHz–0.3 Hz.

3. Results and discussion

3.1. Morphology and structure of the bare and modified TNRs

The FE-SEM images of the bare TNRs (the sample 34-0) are shown in Fig. 1. Fig. 1A and the inset show that the FTO glass is uniformly covered with TiO_2 nanorods, and the density of the nanorod arrays is about 12 per square microns. Fig. 1B shows that the average length of the nanorods is about 3.8 μm, and the nanorods are nearly vertical to the substrate. The XRD patterns of FTO substrate and a bare TiO_2 nanorod array (Fig. 2) show that the diffraction peaks of the TiO_2 nanorod array agree well with the tetragonal rutile phase (JCPDS No. 89-4920), which is consistent with the previous report [6]. Compared to the powder diffraction pattern, the relative intensity of (002) peak is enhanced significantly, which indicates that the nanorods are highly oriented. HR-TEM and SAED patterns of an individual nanorod of the rutile TNRs are shown in Fig. 3. The sharp two-dimensional lattice image and SAED image confirm that the TiO_2 nanorods synthesized directly on FTO glass are single-crystalline. HR-TEM image shows that the nanorod is completely crystalline along its entire length, and the lattice fringes are consistent with the rutile phase, with its interplanar spacing, d_{110} = 3.27 Å and d_{001} = 2.98 Å. The nanorods grow along the [001] direction, which agrees well with the XRD data. TEM image (the inset of Fig. 3A) and the sharp boundary of the nanorod in the HR-TEM image indicate that the side facets of TiO_2 nanorods are smooth, which is a negative factor for dye adsorption.

FE-SEM images of the modified TNRs are shown in Fig. 4. In the top views of these samples, the top surfaces of the nanorods are covered with a large number of TiO_2 nanoparticles and the surfaces become rough. The cross-sectional views show that the nanorods are also covered with a large number of TiO_2 nanoparticles along its entire length. Fig. 4A–F, and I–L shows that with the growth time increasing the diameters of the TiO_2 nanorods covered with TiO_2 nanoparticles increase obviously, which could be attributed to the increase of the amount of the TiO_2 nanoparticles covered on the TiO_2 nanorods. With the same growth time, the TiO_2 nanorod diameter of the samples modified in 0.2 M $TiCl_4$ solution is greater than that of the samples modified in 0.1 M $TiCl_4$ solution. This information indicates that the longer growth time and the greater concentration of $TiCl_4$ solution could lead to a larger amount of TiO_2 nanoparticles covered on the nanorods, which would increase surface area and dye adsorption of the TNRs. These results and deductions have been confirmed through dye adsorption measurement and roughness factor estimation mentioned in the Section 3.2. While in the condition that the concentration of $TiCl_4$ solution is 0.1 M and the growth time is extended to 72 h (Fig. 4F), some pits appear on the surface of the TNRs, where the tops of nanorods

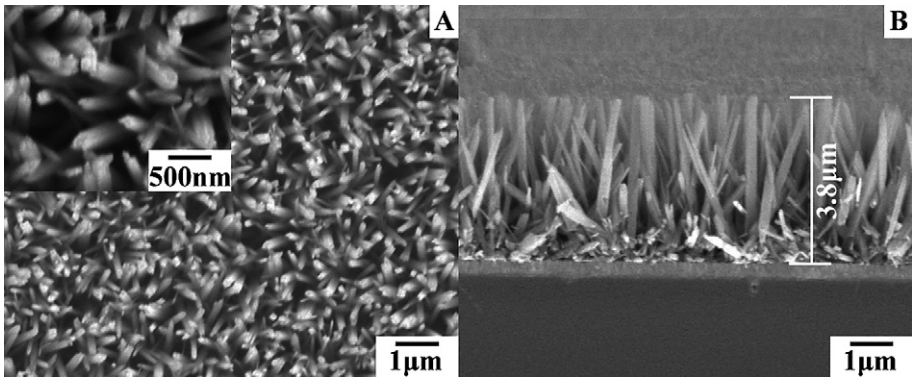

Fig. 1. FE-SEM images of a bare single-crystal TNRs. A) Top view, B) cross-sectional view.

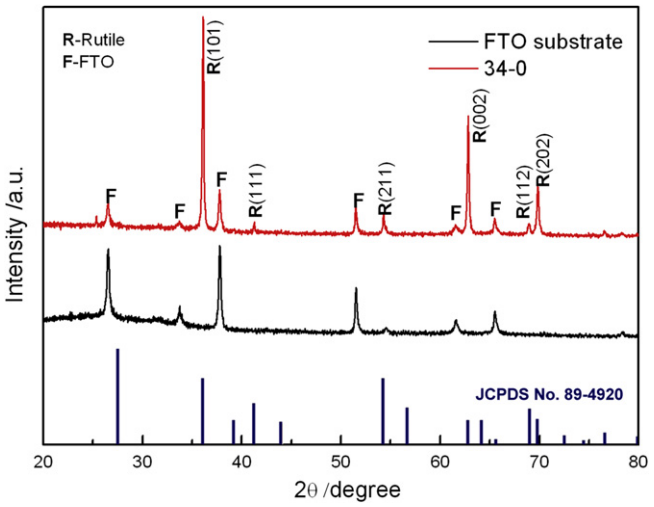

Fig. 2. XRD patterns of FTO glass and a bare single-crystal TNRs.

connect to that of their nearest nanorods, which would affect the performance of DSSCs. In the condition that the concentration of $TiCl_4$ solution is 0.2 M and the growth time is extended to 48 h (Fig. 4L), the gaps between the nanorods are fully filled with TiO_2 nanoparticles, and some cracks appear in the arrays, which would also affect the performance of DSSCs.

The XRD patterns of the bare TNRs and three representative modified TNRs are displayed in Fig. 5. The crystal structures of the four samples are all pure rutile phase, which indicates that the crystal structure of the TiO_2 nanoparticles grown on the TNRs is rutile. Compared to the bare TNRs, the relative intensity of the (002) peaks of the modified TNRs is weak and the other diffraction peaks are enhanced, such as (110), (211), and (112) which could be attributed to the large number of TiO_2 nanoparticles around the oriented nanorods. TEM image (Fig. 6A) of a representative individual nanorod of the modified single-crystal rutile TNRs which has been immersed in 0.1 M $TiCl_4$ solution for 48 h and a lower resolution TEM image (the inset of Fig. 6A) of some individual nanorods of the same sample demonstrate that after the solution growth TiO_2 nanorods are covered with a large number of TiO_2 nanoparticles. The HR-TEM image of some TiO_2 nanoparticles (Fig. 6B) indicates that the TiO_2 nanoparticles are rutile TiO_2. The results of the TEM and HR-TEM are consistent with the XRD and FE-SEM data.

3.2. Performance of DSSCs

In the performance measurement, under each $TiCl_4$ modification condition, six pieces of DSSCs were fabricated and measured. The energy conversion efficiency of each DSSC listed in Table 1 and mentioned in the context is the average value and error of the six pieces of DSSCs.

The J–V curves and photovoltaic parameters of the DSSCs are shown in Fig. 7 and Table 1 respectively. Modification using $TiCl_4$ solution increased the short-circuit current density (J_{sc}), the fill factor (FF) and the energy conversion efficiency (η) of DSSCs (Fig. 7, and Table 1). When the concentration of $TiCl_4$ solution was 0.1 M, the J_{sc} and η increased with the growth time increasing, and they reached the maximum values 8.95 mA cm^{-2} and 4.01 $\pm$ 0.05% respectively when the growth time was 60 h. When the concentration of $TiCl_4$ solution was 0.2 M, the J_{sc} and η increased with the treatment time increasing from 12 to 36 h, the J_{sc} and η reached the maximum values 9.03 mA cm^{-2} and 4.14 $\pm$ 0.07% respectively. However, when the growth time extended to 48 h, the J_{sc} and η decreased, which could be attributed to the cracks appeared in the sample 34-2-48 (Fig. 4L).

IPCE spectra of the cells 34-0, 34-2-12, 34-2-24, 34-2-36 and NP-0 are shown in Fig. 8. The IPCE values of the modified TNRs based DSSCs are much higher than the values of the bare TNRs based DSSC over the whole spectral range (400–800 nm). These results are consistent with the J_{sc} and η of these DSSCs. The values of IPCE of the modified single-crystal rutile TNRs based DSSC 34-2-36 are similar to the values of the P25 nanoparticles based DSSCs NP-0 over the whole spectral range.

Fig. 9 shows the UV–vis absorption spectra of three representative samples 34-0, 34-2-36 and NP-0. The amount of adsorbed dye can be determined from UV–vis absorption spectra by using Lambert–Beer law $A = kbc$, where $k = 4.59 \times 10^4$ L mol^{-1} cm^{-1}, k is the molar extinction coefficient of N719 at 308 nm [24], and the results are listed in Table 1. Brunauer–Emmett–Teller specific surface area (S_{BET}) [25,26] and roughness factor [27,28] are usually used to describe the surface area of the TiO_2 films used for DSSCs. In our investigation, the roughness factor (defined as the total surface area per unit substrate area) is adopted. Assuming that the surface of TiO_2 films is covered with a monolayer of dye N719, and the coverage of dye N719 is 16 nm^2/molecule [27,28], the roughness factors of different films have been estimated according to the amount of adsorbed dye and listed in Table 1, too. It can be seen that the adsorbed dye and roughness factor of TNRs both are increased with the increase of $TiCl_4$ concentration and growth time. This

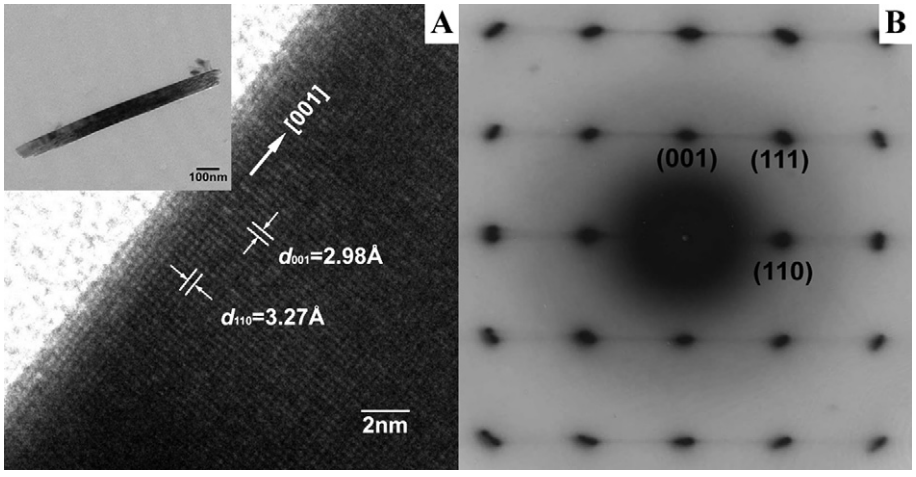

Fig. 3. A) HR-TEM image and B) SAED image of an individual nanorod of the single-crystal rutile TNRs.

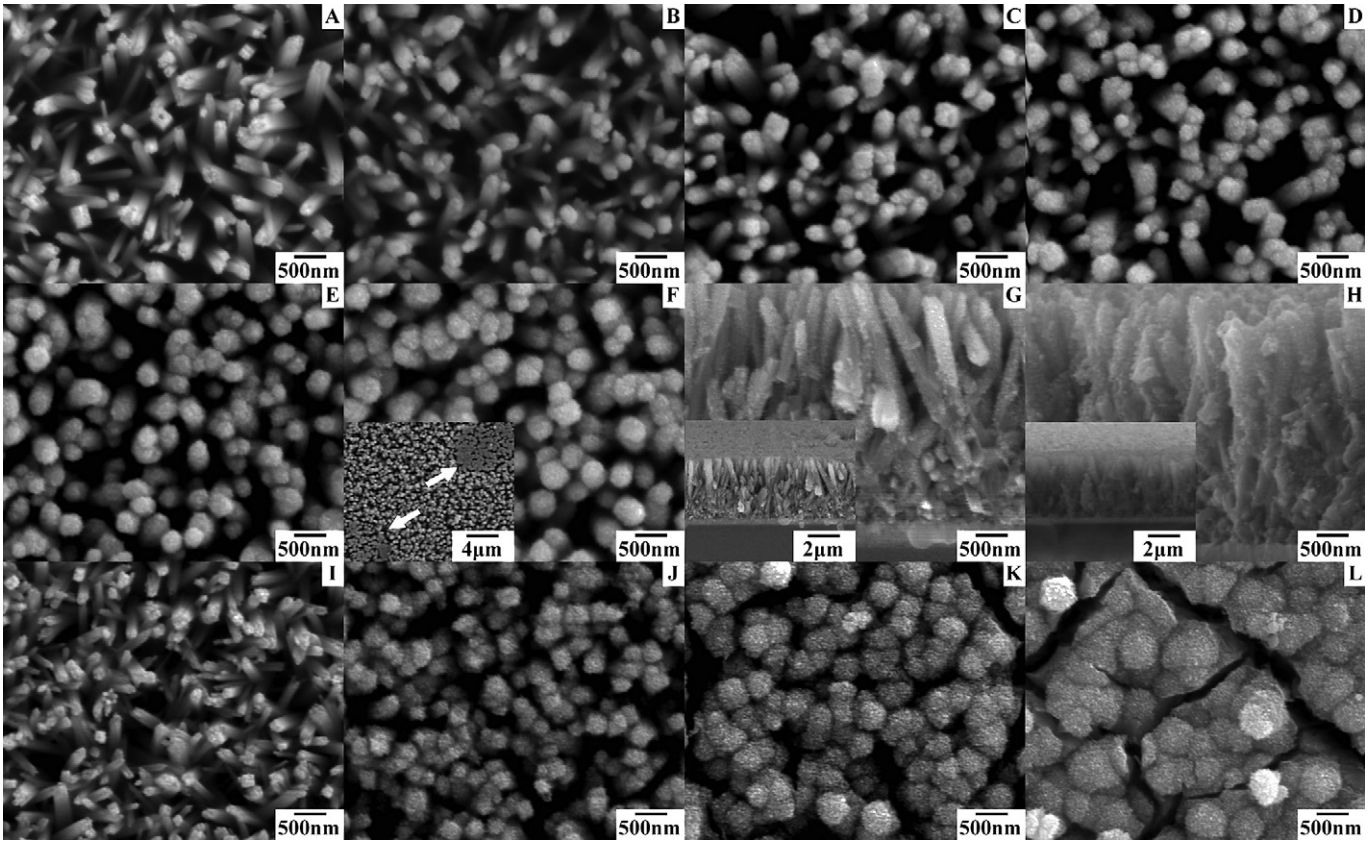

Fig. 4. FE-SEM images of the samples which were modified through $TiCl_4$ solution growth: A), B), C), D), E), and F) are top views of the modified single-crystal rutile TNRs which were immersed in 0.1 M $TiCl_4$ solution for 12, 24, 36, 48, 60, and 72 h respectively, G) and the inset are cross-sectional views of the sample 34-1-24. I), J), K), and L) are top views of the modified single-crystal rutile TNRs which were immersed in 0.2 M $TiCl_4$ solution for 12, 24, 36, and 48 h respectively, H) and the inset are cross-sectional views of the sample 34-2-24.

result is consistent with FE-SEM images of Fig. 4. The increase of the amount of the TiO_2 nanoparticles covered on the TiO_2 nanorods arrays leads to the increase of the roughness factor and surface area, and then increases dye adsorption of the TNRs. The increase of dye adsorption could increase the amount of the photogenerated electrons, and then increases short-circuit current and energy conversion efficiency of the DSSCs. When the concentration of $TiCl_4$ solution is 0.2 M and the growth time is 36 h, dye adsorption of the modified single-crystal rutile TNRs increases by 90%, the J_{sc} increases by over 5 times, and the η increases by about 7 times. Besides the reasons mentioned above, the passivation layer composed of TiO_2 nanoparticles formed on the FTO glass in the modification process could also increase the J_{sc} and η of the DSSCs. The passivation layer would prevent the direct contact between the electrolyte and the electrons passing through the FTO electrode, which would reduce the recombination between the electrons and the I_3^- ions in the electrolyte.

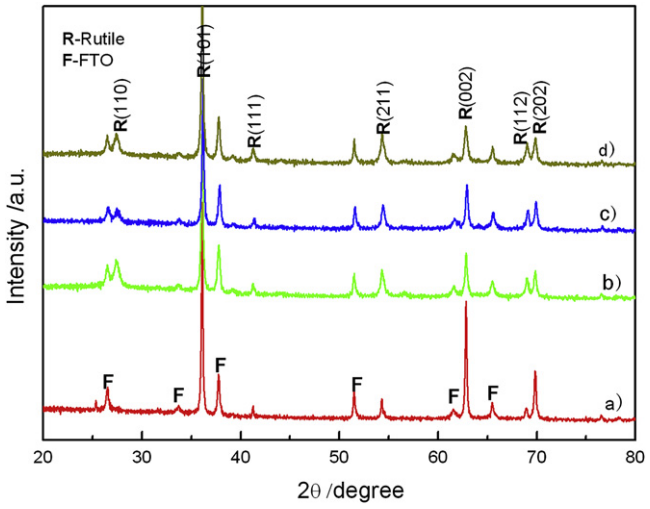

Fig. 5. XRD patterns of a) a bare single-crystal rutile TNRs, and the modified single-crystal rutile TNRs which were immersed in b) 0.1 M $TiCl_4$ solution for 48 h, c) 0.2 M $TiCl_4$ solution for 24 h, and d) 0.2 M $TiCl_4$ solution for 36 h.

However, it is surprising that the amounts of adsorbed dye and roughness factors of the samples 34-1-12, 34-1-24, and 34-2-12 are all smaller than that of the bare TNRs 34-0. The $TiCl_4$ solution growth parameters of the samples 34-1-12, 34-1-24, and 34-2-12 are similar to that of the often used $TiCl_4$ treatment method for TiO_2 nanoparticles based DSSCs reported in the previous publications [29,30]. The previous investigation [29] revealed that after immersion in the $TiCl_4$ solution, new layers with piled-needle-like shapes are produced on the TiO_2 surface, which leads to a significant increase of surface area. However, after annealing the piled-needle-like structure disappears, which makes the surface area of the electrode smaller than that of the sample without any treatment. The investigation reported in the previous publication [12] revealed that after immersion in the $TiCl_4$ solution, each TiO_2 nanorod of single-crystal rutile TNRs is enclosed by TiO_2 nanobranches. According to the two investigations mentioned above and our investigation, a reasonable inference could be obtained. After immersion in $TiCl_4$ solution each TiO_2 nanorod is enclosed by

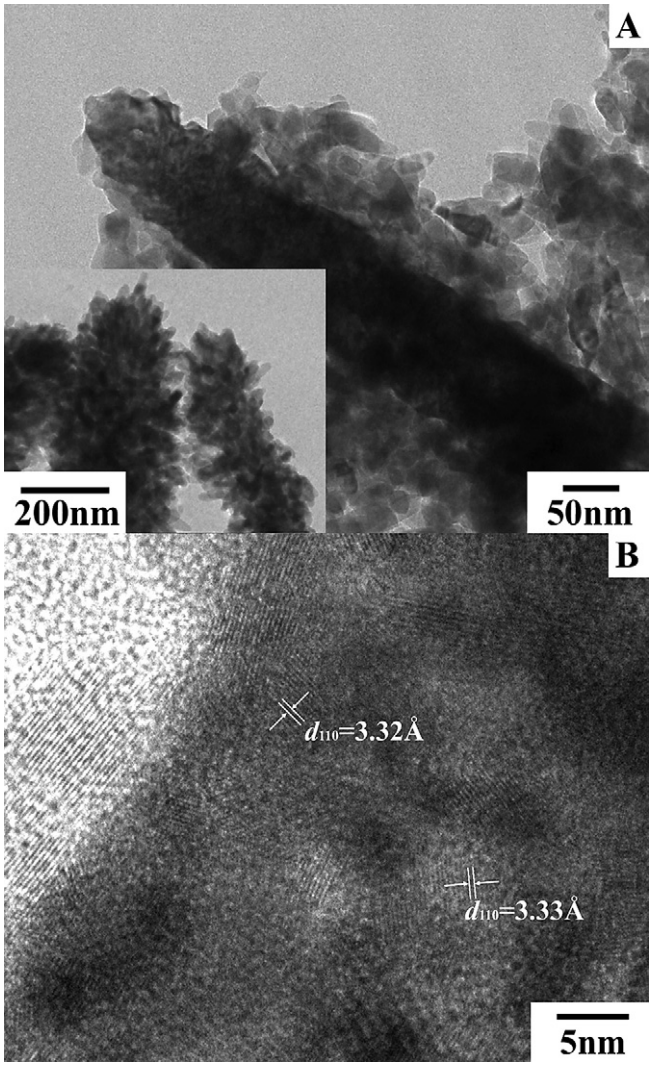

Fig. 6. A) TEM image of a representative individual nanorod of the modified single-crystal rutile TNRs which was immersed in 0.1 M $TiCl_4$ solution for 48 h and the inset is a lower resolution TEM image of some individual nanorods of the same sample, B) HR-TEM image of some TiO_2 nanoparticles attached to the surface of an individual nanorod of the same sample.

TiO_2 nano-branches, annealing makes the TiO_2 nano-branches convert to thin films and cover on the surface of TiO_2 nanorods when the concentration of $TiCl_4$ solution is 0.1 M, growth time is 12 or 24 h or when the concentration is 0.2 M, growth time is 12 h. As a result, the short nanorods disorderly and closely located in the bottom of the TNRs (Fig. 1B) grow bigger and connect to each other, and then decrease the surface area of the TNRs, which is a negative factor for the increase of the surface area of the TNRs. At the same time, the orderly aligned long nanorods would grow bigger, which would lead to the increase of the surface area of the TNRs. Compared to the negative factor mentioned above the increase factor is a minor factor. Therefore, the surface areas and the roughness factors of the samples 34-1-12, 34-1-24, and 34-2-12 are smaller than that of the bare TNRs. With the growth time extending, the increase factor for the surface area of the TNRs increases and becomes a major factor. After annealing TiO_2 nano-branches enclosed on the surface of nanorods would convert to TiO_2 nanoparticles, and then increases the surface area of the TNRs significantly.

The efficiency of the cell NP-0 is similar to the cell 34-2-36, but the amount of adsorbed N719 of the sample NP-0 was 4.5 times

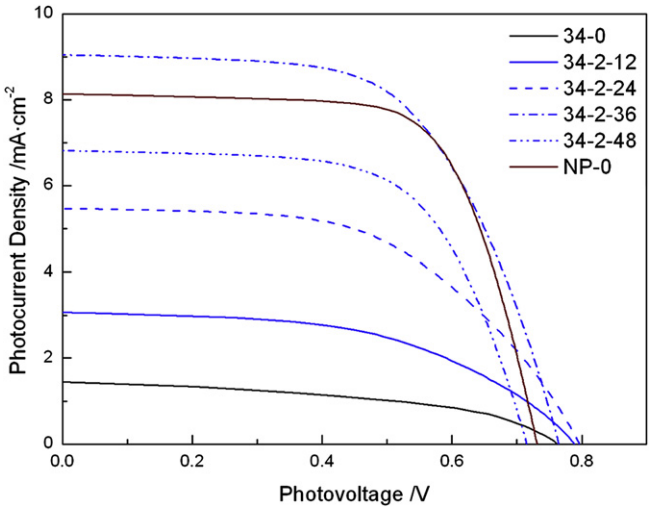

Fig. 7. Photocurrent–photovoltage characteristics of DSSCs based on bare single-crystal rutile TNRs, modified single-crystal rutile TNRs which were modified using 0.2 M $TiCl_4$ solution, and a P25 TiO_2 nanoparticles film.

greater than that of the sample 34-2-36. This information indicates that the modified single-crystal rutile TNRs have higher light-harvesting efficiency, which could be confirmed by UV–vis DRS and digital photographs of the films NP-0 and 34-2-36 shown in Fig. 10. In the UV–vis DRS, the significant increase in the absorption at wavelengths shorter than 400 nm is attributed to the intrinsic band gap absorption of TiO_2, and the difference between absorption edges of the samples NP-0 and 34-2-36 is ascribed to the different crystal phases of the samples. The visible light absorption of the sample 34-2-36 is higher than that of the sample NP-0, which indicates that the light-harvesting capability of the modified TNRs is higher than that of P25 TiO_2 nanoparticles film. The digital photographs (the inset of Fig. 10) show that the P25 TiO_2 nanoparticles coated FTO substrate is nearly transparent, but the modified single-crystal rutile TNRs coated FTO glass is opaque, which confirm the results obtained in UV–vis DRS. To achieve similar energy conversion efficiencies, the amount of adsorbed dye of the modified single-crystal rutile TNRs based DSSCs is far less than that of P25 TiO_2 nanoparticles base DSSCs.

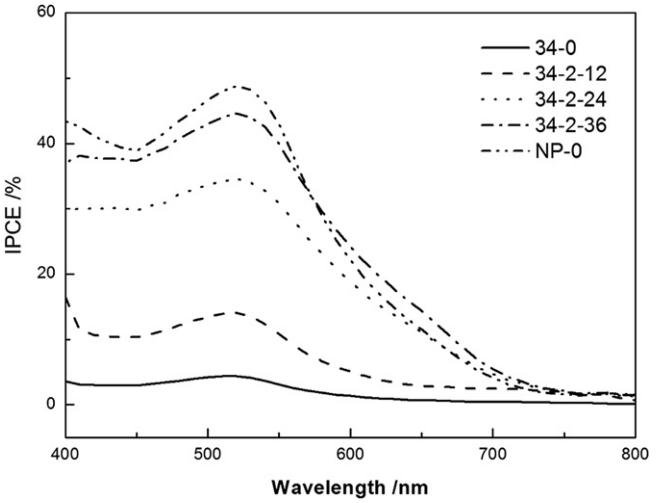

Fig. 8. IPCE spectra of DSSCs based on bare single-crystal rutile TNRs, modified single-crystal rutile TNRs, and a P25 TiO_2 nanoparticles film.

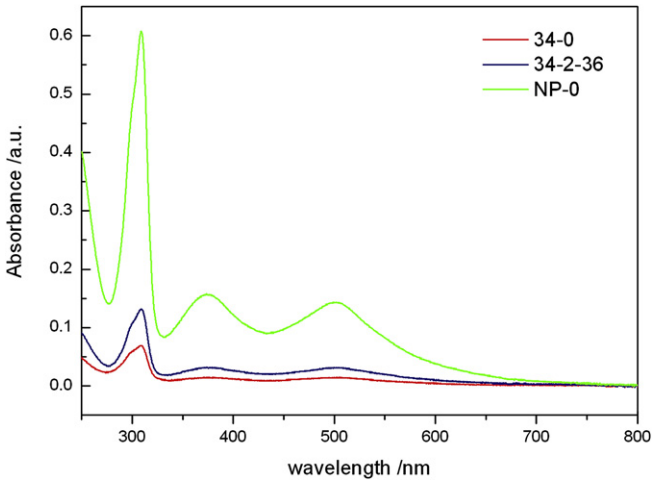

Fig. 9. UV–vis absorption spectra of N719 desorbed from 1.5 cm^2 sensitized electrodes 34-0, 34-2-36 and NP-0, the desorbed N719 dissolved in 10 mL of 0.2 M NaOH solution.

3.3. Electron transport properties

To compare electron transport properties in two photoanodes with different morphologies fairly, the two photoanodes should have equal roughness factor and porosity, equal photoanode thickness, equal photocurrent or equal efficiencies [13]. The energy conversion efficiency of the cell NP-0 used for comparison was 4.07 ± 0.07%, which is similar to the efficiency of the cell 34-2-36. The comparison between the bare and modified TNRs was used to determine the effect of TiO_2 nanoparticles covered on the TNRs on the electron transport of TNRs. The electron transport properties of the three cells 34-0, 34-2-36 and NP-0 were compared to determine the difference between P25 TiO_2 nanoparticles film and single-crystal rutile TNRs in electron transport properties. In order to make the comparisons practical, IMPS and IMVS measurements of all DSSCs were carried out under the same illumination condition, the illumination power density was fixed to 8 mW cm^{-2}. The IMPS and IMVS responses of the three DSSCs are shown in Fig. 11. The inset of Fig. 11A is the IMPS response of the cell 34-0, and the disordered points in the left of the curve are due to the small photocurrent of the cell 34-0. The electron transport time constant τ_d can be evaluated using the equation $\tau_d = 1/2\pi f_{IMPS}$ [15], where f_{IMPS} is the characteristic frequency at the minimum of imaginary IMPS. The electron recombination lifetime constant τ_n can be evaluated using the equation $\tau_n = 1/2\pi f_{IMVS}$ [15], where f_{IMVS} is the characteristic frequency at the minimum of imaginary IMVS. The charge-collection efficiency can be evaluated using the equation $\eta_{cc} = 1 - \tau_d/\tau_n$ [15]. The electron transport characteristics obtained from IMPS and IMVS measurements were listed in Table 2.

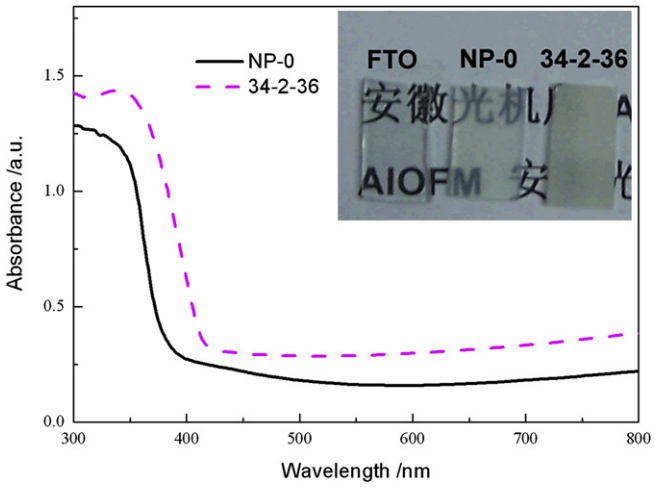

Fig. 10. UV–vis diffuse reflection spectra of an FTO substrate coated with 4.9 ± 0.2 μm thick P25 TiO2 nanoparticles film (NP-0) and an FTO substrate coated with 3.8 ± 0.04 μm thick modified single-crystal rutile TNRs (34-2-36), the inset is their digital photographs.

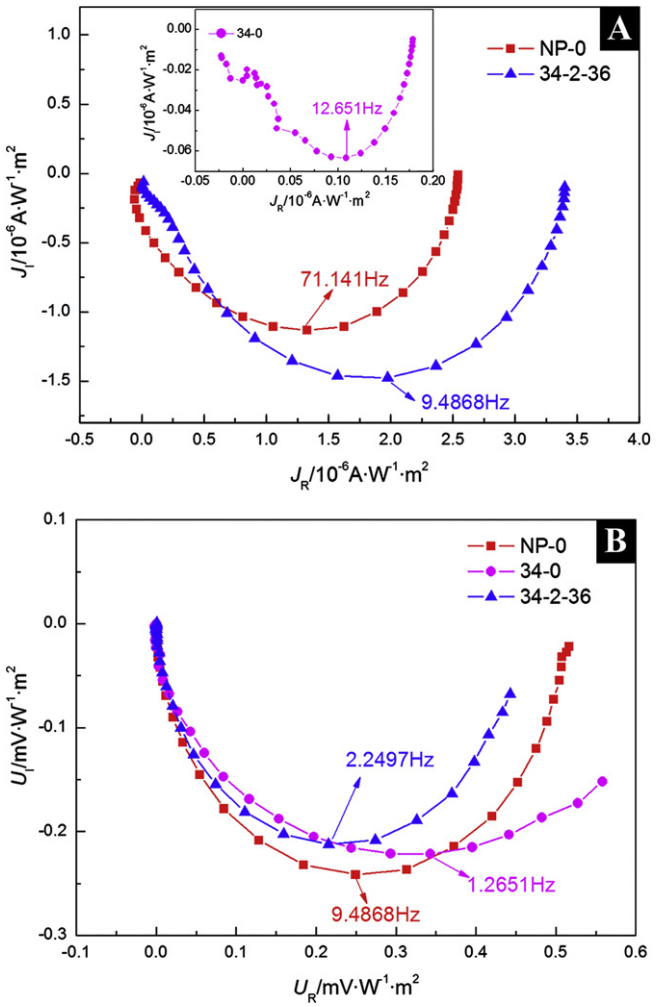

Fig. 11. A) IMPS and B) IMVS of the DSSCs based on P25 TiO_2 nanoparticles film NP-0, bare single-crystal rutile TNRs 34-0 and the modified single-crystal rutile TNRs 34-2-36.

The electron transport time τ_d and the electron recombination lifetime τ_n of the modified single-crystal rutile TNRs are slightly longer and obviously shorter than that of the bare single-crystal rutile TNRs respectively. The charge-collection efficiency η_{cc} was reduced from 90% to 76.29% after $TiCl_4$ modification. This information indicates that $TiCl_4$ modification reduces the electron transport rate, the electron recombination lifetime τ_n and the charge-collection efficiency η_{cc} of the single-crystal rutile TNRs obviously, which is a negative factor for the performance of the single-crystal rutile TNRs based DSSCs. Compared to the increase of the surface area, dye adsorption and the short-circuit current caused by $TiCl_4$ modification, this negative factor is minor.

Compared to the P25 TiO_2 nanoparticles film based cell NP-0, the electron transport time τ_d of the bare and modified TNRs based cells 34-0 and 34-2-36 are about six and eight times larger

Table 2
Electron transport properties of the DSSCs based on bare single-crystal rutile TNRs 34-0, modified single-crystal rutile TNRs 34-2-36 and P25 TiO_2 nanoparticles film NP-0.

Sample	f_{IMPS} (Hz)	τ_d (s)	f_{IMVS} (Hz)	τ_n (s)	η_{cc} (%)
34-0	12.651	0.0126	1.2651	0.1258	90.00
34-2-36	9.4868	0.0168	2.2497	0.0707	76.29
NP-0	71.141	0.0022	9.4868	0.0168	86.66

respectively, which indicates that the electron transport rate of the bare and modified TNRs is much slower than that of the P25 TiO_2 nanoparticles film. This result is contrary to the expectations and the result obtained by Enache-Pommer [13], but it is close to the result of the comparison between anatase TiO_2 nanoparticles film and rutile TiO_2 nanoparticles film investigated by Park [31] which showed that the electron transport rate in rutile TiO_2 nanoparticles film is one order of magnitude slower than in anatase TiO_2 nanoparticles film. The single-crystal rutile TNRs doesn't show any superiority in the electron transport than P25 TiO_2 nanoparticles film. The results indicate that although one-dimensional nanostructure is advantageous in electron transport, but the rutile phase of the TiO_2 nanorod is a negative factor for electron transport, and the latter is the decisive factor for electron transport rate. If single-crystal anatase TNRs could be synthesized and used as photoanodes of DSSCs, the advantages of the fast electron transport rate in the single-crystal TNRs would become realizable.

The electron recombination lifetime τ_n of the P25 TiO_2 nanoparticles based DSSC NP-0, the typical modified TNRs based DSSC 34-2-36, and the bare TNRs based DSSC 34-0 are 0.0168, 0.0707, and 0.1258 s respectively. Compared to P25 TiO_2 nanoparticles based DSSCs, the electron recombination lifetime τ_n of the DSSCs based on bare and modified TNRs increased significantly. According to the equation $\eta_{cc} = 1 - \tau_d/\tau_n$ [15], the longer electron recombination lifetime would increase the charge-collection efficiency. The charge-collection efficiencies of the three DSSCs were listed in Table 2. Compared to the other two DSSCs, the highest charge-collection efficiency of the bare single-crystal rutile TNRs based DSSC can be attributed to the longest electron recombination lifetime. But its energy conversion efficiency is the lowest in the three DSSCs, which could be attributed to its small surface area and the lower dye adsorption. The surface area and dye adsorption of the modified single-crystal rutile TNRs were increased significantly, but the modified TNRs contained a large number of rutile TiO_2 nanoparticles, rutile TiO_2 nanoparticles are disadvantageous in electron transport [27] and electron recombination lifetime, and then the charge-collection efficiency of the modified TNRs is slightly lower than that of P25 TiO_2 nanoparticles film and bare TNRs. But the increased dye adsorption improves the energy conversion efficiency significantly.

The electron transport rate of bare and modified single-crystal rutile TNRs is slower than that of P25 TiO_2 nanoparticles film. But the increase of the electron recombination lifetime τ_n of bare and modified single-crystal rutile TNRs compensates for the slow electron transport rate, and makes the charge-collection efficiency of bare single-crystal rutile TNRs based DSSCs be similar and the charge-collection efficiency of modified single-crystal rutile TNRs based DSSCs be slightly lower to that of P25 TiO_2 nanoparticles based DSSCs.

4. Conclusion

Through $TiCl_4$ solution growth, a large number of rutile TiO_2 nanoparticles are synthesized on the surface of single-crystal rutile TiO_2 nanorods. The surface area and dye adsorption of the single-crystal rutile TNRs are increased significantly, the J_{sc} and η of single-crystal rutile TNRs based DSSCs are increased from 1.47 mA cm^{-2} and 0.52 ± 0.03% to 9.03 mA cm^{-2} and 4.14 ± 0.07% respectively.

Compared to P25 TiO_2 nanoparticles based DSSCs, the light-harvesting efficiency of the single-crystal rutile TNRs based DSSCs is higher. To obtain similar energy conversion efficiencies, the amount of adsorbed dye of the modified single-crystal rutile TNRs based DSSCs is far less than that of P25 TiO_2 nanoparticles based DSSCs.

The electron transport rate of bare and modified single-crystal rutile TNRs is slower than that of P25 TiO_2 nanoparticles film, but their electron recombination lifetime τ_n is longer than that of P25 TiO_2 nanoparticles film, and the charge-collection efficiencies of bare and modified single-crystal rutile TNRs based DSSCs are similar to that of P25 TiO_2 nanoparticles based DSSCs.

Further works could be done to improve the performance of single-crystal TNRs based DSSCs. Firstly, try to synthesize single-crystal anatase TNRs. Secondly, prepare thicker single-crystal rutile TNRs composed of longer nanorods. Thirdly, continue to optimize the modification parameters of $TiCl_4$ solution growth.

Acknowledgments

This work was supported by the National Natural Science Foundation of China (Grant No. 51172237), the National Basic Research Program of China (Grant No. 2011CBA00700), the National High Technology Research and Development Program of China (Grant No. 2011AA050527), Anhui Provincial International Science and Technology Cooperation Program (Grant No. 10080703021), and Anhui Provincial Key Lab of Photonics Devices and Materials.

References

[1] B. O'Regan, M. Grätzel, Nature 353 (1991) 737–740.
[2] M. Grätzel, Acc. Chem. Res. 42 (2009) 1788–1798.
[3] C.Y. Chen, M.K. Wang, J.Y. Li, N. Pootrakulchote, L. Alibabaei, C.H. Ngoc-Le, J.D. Decoppet, J.-H. Tsai, C. Grätzel, C.G. Wu, S.M. Zakeeruddin, M. Grätzel, ACS Nano 3 (2009) 3103–3109.
[4] A. Yella, H.W. Lee, H.N. Tsao, C. Yi, A.K. Chandiran, Md.K. Nazeeruddin, E.W.-G. Diau, C.Y. Yeh, S.M. Zakeeruddin, M. Grätzel, Science 334 (2011) 629–634.
[5] M.A. Green, K. Emery, Y. Hishikawa, W. Warta, E.D. Dunlop, Prog. Photovolt. Res. Appl. 20 (2012) 12–20.
[6] B. Liu, E.S. Aydil, J. Am. Chem. Soc. 131 (2009) 3985–3990.
[7] Y. Zhang, Y. Gao, X.H. Xia, Q.R. Deng, M.L. Guo, L. Wan, G. Shao, Mater. Lett. 64 (2010) 1614–1617.
[8] R.H. Tao, J.M. Wu, H.X. Xue, X.M. Song, X. Pan, X.Q. Fang, X.D. Fang, S.Y. Dai, J. Power Sources 195 (2010) 2989–2995.
[9] X.J. Feng, K. Shankar, O.K. Varghese, M. Paulose, T.J. Latempa, C.A. Grimes, Nano Lett. 8 (2008) 3781–3786.
[10] H.E. Wang, Z.H. Chen, Y.H. Leung, C.Y. Luan, C.P. Liu, Y.B. Tang, C. Yan, W.J. Zhang, J.A. Zapien, I. Bello, S.T. Lee, Appl. Phys. Lett. 96 (2010) 263104.1–263104.3.
[11] A. Kumar, A.R. Madaria, C.W. Zhou, J. Phys. Chem. C 114 (2010) 7787–7792.
[12] H. Wang, Y.S. Bai, Q. Wu, W. Zhou, H. Zhang, J.H. Li, L. Guo, Phys. Chem. Chem. Phys. 13 (2011) 7008–7013.
[13] E. Enache-Pommer, B. Liu, E.S. Aydil, Phys. Chem. Chem. Phys. 11 (2009) 9648–9652.
[14] M.J. Yang, B. Ding, S.W. Lee, J.K. Lee, J. Phys. Chem. C 115 (2011) 14534–14541.
[15] Q.L. Huang, G. Zhou, L. Fang, L.P. Hu, Z.S. Wang, Energy Environ. Sci. 4 (2011) 2145–2151.
[16] L. Dloczik, O. Ileperuma, I. Lauermann, L.M. Peter, E.A. Ponomarev, G. Redmond, N.J. Shaw, I. Uhlendorf, J. Phys. Chem. B 101 (1997) 10281–10289.
[17] G. Schlichtho1rl, N.G. Park, A.J. Frank, J. Phys. Chem. B 103 (1999) 782–791.
[18] J. Kru1ger, R. Plass, M. Grätzel, P.J. Cameron, L.M. Peter, J. Phys. Chem. B 107 (2003) 7536–7539.
[19] J. van de Lagemaat, N.G. Park, A.J. Frank, J. Phys. Chem. B 104 (2000) 2044–2052.
[20] B.H. Lee, M.Y. Song, S.Y. Jang, S.M. Jo, S.Y. Kwak, D.Y. Kim, J. Phys. Chem. C 113 (2009) 21453–21457.
[21] T. Oekermann, D.S. Zhang, T. Yoshida, H. Minoura, J. Phys. Chem. B 108 (2004) 2227–2235.
[22] J.G. Yu, J.J. Fan, B. Cheng, J. Power Sources 196 (2011) 7891–7898.
[23] J.J. Fan, S.W. Liu, J.G. Yu, J. Mater. Chem. 22 (2012) 17027–17036.

[24] M.K. Nazeeruddin, S.M. Zakeeruddin, R. Humphry-Baker, M. Jirousek, P. Liska, N. Vlachopoulos, V. Shklover, Christian-H. Fischer, M. Grätzel, Inorg. Chem. 38 (1999) 6298–6305.
[25] J.G. Yu, J.J. Fan, L. Zhao, Electrochim. Acta 55 (2010) 597–602.
[26] J.G. Yu, J.J. Fan, K.L. Lv, Nanoscale 2 (2010) 2144–2149.
[27] M. Grätzel, Pure Appl. Chem. 73 (2001) 459–467.
[28] B. Tan, Y.Y. Wu, J. Phys. Chem. B 110 (2006) 15932–15938.
[29] S. Kambe, S. Nakade, Y. Wada, T. Kitamura, S. Yanagida, J. Mater. Chem. 12 (2002) 723–728.
[30] F.J. Knorr, D.S. Zhang, J.L. McHale, Langmuir 23 (2007) 8686–8690.
[31] N.G. Park, J. van de Lagemaat, A.J. Frank, J. Phys. Chem. B 104 (2000) 8989–8994.